Surface atomic and chemical structure of relaxor Sr0.63Ba0.37Nb2O6(001)

J. L. Wang, B. Vilquin, B. Gautier, G. Dezanneau, N. Barrett

Surface atomic and chemical structure of relaxor Sr0.63Ba0.37Nb2O6(001)

J. L. Wang, B. Vilquin, B. Gautier, G. Dezanneau, and N. Barrett

Citation: Applied Physics Letters **106**, 242901 (2015); doi: 10.1063/1.4922773
View online: http://dx.doi.org/10.1063/1.4922773
View Table of Contents: http://scitation.aip.org/content/aip/journal/apl/106/24?ver=pdfcov
Published by the AIP Publishing

Surface atomic and chemical structure of relaxor $Sr_{0.63}Ba_{0.37}Nb_2O_6(001)$

J. L. Wang,[1] B. Vilquin,[2] B. Gautier,[3] G. Dezanneau,[4] and N. Barrett[1,a)]
[1]*Service de Physique de Condensé, DSM/IRAMIS/SPEC, CNRS UMR 3680, CEA Saclay, 91191 Gif sur Yvette Cedex, France*
[2]*Université de Lyon, École Centrale de Lyon, Institut des Nanotechnologies de Lyon, F-69134 Ecully Cedex, France*
[3]*Université de Lyon, INSA Lyon, Institut des Nanotechnologies de Lyon, F-69621 Villeurbanne Cedex, France*
[4]*Laboratoire Structure, Propriétés et Modélisation des Solides, École CentraleSupelec, CNRS, Grande Voie des Vignes, F-92295 Châtenay-Malabry Cedex, France*

(Received 29 April 2015; accepted 8 June 2015; published online 19 June 2015)

The surface atomic and chemical structures of a $Sr_{0.63}Ba_{0.37}Nb_2O_6(001)$ single crystal are studied using the low-energy electron diffraction (LEED) and X-ray photoelectron spectroscopy. Sharp, well-defined LEED patterns are observed, consisting of the superposition of two surface reconstructions, $(\sqrt{5}\times\sqrt{5})R26.6°$ and $(5\sqrt{2}\times\sqrt{2})R45°$, probably due to long-range ordering of the alkaline earth metal vacancies in A1 or A2 sites. The Sr/Ba stoichiometry is determined by high-resolution X-ray photoelectron spectroscopy. The Sr 3d core level has 2 components corresponding to the 12- and 15-fold coordinated A1 and A2 sites. The Ba 3d core level has only one component, consistent with the A2 site occupancy. The long-range order of the cation vacancies implies that it is rather the Sr/Ba occupancy of the A2 sites which is responsible for the local random fields at the origin of the relaxor behavior. © *2015 AIP Publishing LLC*. [http://dx.doi.org/10.1063/1.4922773]

Tetragonal tungsten bronzes have been widely investigated because of their outstanding pyroelectric, piezoelectric, and nonlinear optical properties.[1] In particular, much interest has been devoted to $Sr_x\ Ba_{1-x}\ Nb_2O_6$ (SBN100x) due to its excellent electro-optical properties.[2–6] SBN is a uniaxial ferroelectric with spontaneous polarization along the c-axis and shows relaxor behavior as the Sr content increases.[7] The Curie temperature, dielectric constant, and P-E hysteresis can be varied by changing the Sr/Ba atomic ratio in the range of $0.25 < x < 0.75$.[8] For $x > 0.6$, typical relaxor behavior is observed with a broad frequency dependent peak of the dielectric permittivity versus temperature. The relaxor behavior is believed to be due to quenched random fields (RFs) resulting from randomly distributed cation vacancies on the A type sites.[9] A better understanding of how cation chemistry influences the relaxor properties is desirable to optimize material design.

The unit cell can be described by the general structural formula $[(A1)_2(A2)_4C_4][(B1)_2(B2)_8]O_{30}$, where A, B, and C represent the different cation sites. The narrowest, triangular channels (type C) with 9-fold oxygen coordination sites are too small to contain either Sr or Ba. The intermediate tetragonal channels (A1) with 12-fold oxygen coordination are occupied only by the Sr atoms while the largest, pentagonal channels (A2) with 15-fold oxygen coordination sites can be filled by Ba or Sr atoms.[10,11] The ferroelectric polarization is determined mainly by the distortion of the NbO_6 octahedra; whereas variation of the [Sr]/[Ba] atomic ratio shifts the temperature of the FE to PE phase transition, changes the permittivity, and modifies the relaxor properties of SBN.[11] Regardless of the [Sr]/[Ba] ratio, 1/6 of the A (=A1 + A2) sites are empty,[12] whereas the B1 and B2 sites are fully occupied by Nb atoms.

Electric charge disorder can create local RFs.[13] X-ray diffraction (XRD) has suggested that the local structural modifications induced by the isovalent Sr/Ba occupancy of the A2 site may be responsible for the charge disorder.[14] Chernaya *et al*. have shown that the displacement of the Sr atom from the mirror plane in the pentagonal A2 site is correlated with the relaxor properties.[10] It is therefore of interest to study more closely the local and long-range chemical order in SBN. Here, we report an experimental study of the SBN (001) single crystal surface. The surface atomic structure is determined using low-energy electron diffraction (LEED) and strongly suggests long-range ordering of cation vacancies. X-ray photoelectron spectroscopy (XPS) is used to determine the surface Sr/Ba stoichiometry and chemical environment of each atomic species. Piezo response force microscopy (PFM) confirms the existence and size of polar regions characteristic of relaxor SBN.

The $10\times10\times0.6\,mm^3$ SBN (001) single crystal was furnished by Pi-KEM. To eliminate surface carbon contamination, the sample was ozone-cleaned by a short, 10 min exposure to UV light in air before being introduced into the ultra-high vacuum (UHV) setup. Then, it was annealed successively at 300, 500, and 700 °C for 1 h to remove residual contamination on the surface.[15] LEED and XPS analyses were performed *in-situ* in the same UHV setup, with a base pressure of 2×10^{-10} mbar. XPS was carried out using a monochromatic Al Kα (1486.7 eV) X-ray source (Omicron Nanotechnology GmbH). The overall energy resolution (photons and spectrometer) was 0.35 eV. PFM employed a NT-MDT Ntegra AFM for the phase imaging at 6 V ac and 3.7 kHz, using a Co/Cr tip and a 1–10 N/m stiffness. Dielectric measurements were performed on a 2-point measurement setup with cryo-furnace and possibilities to control

a)Author to whom correspondence should be addressed. Electronic mail: nick.barrett@cea.fr

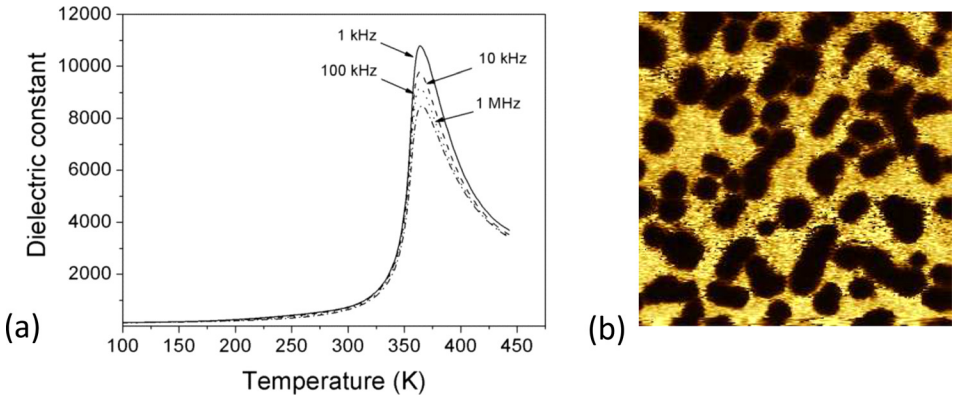

FIG. 1. (a) Dielectric response of SBN single crystal for frequencies between 1 kHz and 1 MHz. The Curie temperature is 360 K. (b) PFM phase response of SBN surface. Phase scale: 180° from black to white.

the temperature between 80 and 500 K. The impedance was measured at frequencies varying between 1 kHz and 1 MHz (12 frequency per decade) with a Agilent 4294 A impedance analyser. The excitation voltage was 200 mV. XRD was performed with a 4 circle diffractometer.

The temperature dependence of the dielectric constant for frequencies from 1 kHz to 1 MHz is plotted in Fig. 1(a). The Curie temperature, as deduced from the 1 kHz curve, is 360 K, which corresponds to SBN61.[16] The single crystal X-ray diffraction gave $a = 3.9324$ and $c = 12.4526$ Å, which corresponds to SBN63. The $2 \times 2\ \mu m^2$ PFM phase image is shown in Fig. 1(b). There is clear contrast that could correspond to the expected polar nano-regions (PNRs). The phase shift is close to 180° as expected from domains with opposite polarization. The measured polarization pattern has no obvious relationship with the topography (not shown). Analysis of 50 such polar regions gives an average size of $0.151 \pm 0.023\ \mu m^2$, in good agreement with previous results for SBN61-SBN75.[9] The absence of electro-mechanical response in the bright areas of Fig. 1(b) corresponds to the piezo-inactive areas observed by Shvartsman *et al.*[9] A rather high amplitude (6 V) has been used for the alternating voltage during PFM imaging, in order to enhance the signal to noise ratio. For our 600 μm thick crystal, this corresponds to an electric field of 100 V/cm, slightly increased by the tip effect, but not so that it reaches the coercive field. Therefore, PFM imaging has no influence on the genuine domain configuration, and imaging has been performed several times with no contrast change.

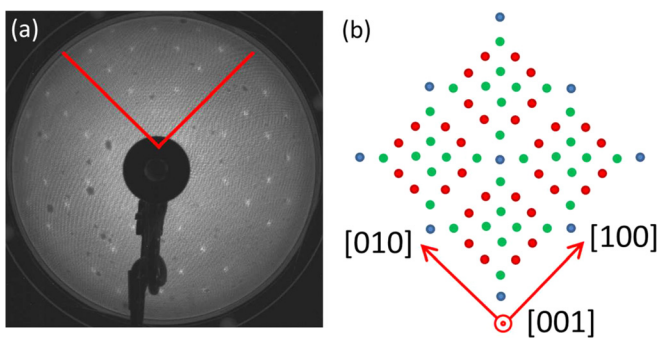

FIG. 2. (a) LEED image on SBN(001) single crystal surfaces at 45 eV. (b) Schematic LEED diffraction pattern showing superposition of two patterns, $(\sqrt{5} \times \sqrt{5})$R26.6° (red) and $(5\sqrt{2} \times \sqrt{2})$R45° (green). The common points are marked by blue color.

Figure 2(a) presents the LEED pattern acquired at 45 eV to maximize surface sensitivity. The well-defined spots show the square symmetry structure of the SBN(001) surface and reveal the presence of long-range, ordered reconstruction. The LEED spots are perfectly reproduced by the schematic presented in Fig. 2(b), obtained by the superposition of two reconstructions: $(\sqrt{5} \times \sqrt{5})$R26.6° (red) and $(5\sqrt{2} \times \sqrt{2})$R45° (green)[17,18] which can easily be formed by an ordered distribution of the empty A-type sites, as shown in Fig. 3. The 1/6 vacant A-sites is perfectly respected by the two surface reconstructions based on cation vacancy ordering. Long-range ordering of A-site vacancies is not compatible with the random

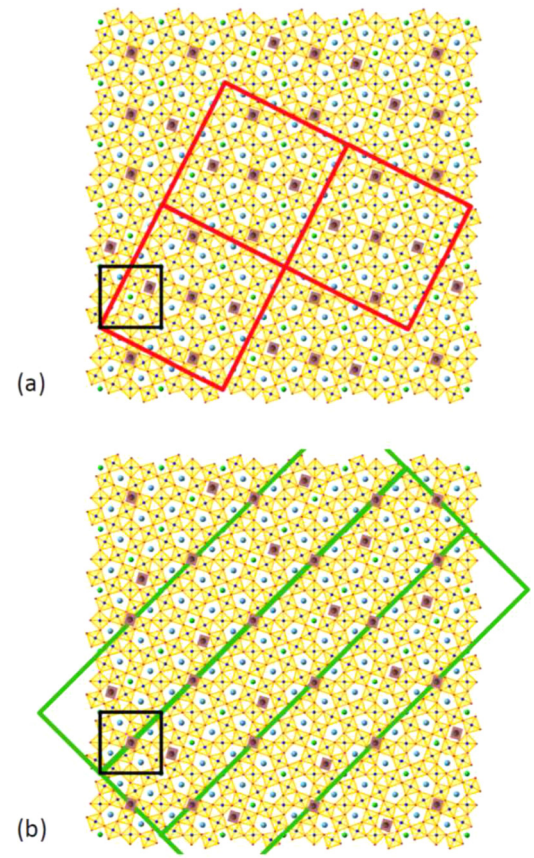

FIG. 3. Schematics of the $(\sqrt{5} \times \sqrt{5})$R26.6° (a) and $(5\sqrt{2} \times \sqrt{2})$R45° (b) reconstructions due to different cation vacancy distributions. Three unit cells are shown for each reconstruction. The bulk cation vacancy concentration of 1/6 is respected as are the A1/A2 site ratios in the reconstructed unit cells. Vacancy sites are indicated by the small shaded squares. The SBN (1 × 1) unit cell is the small (black) square.

distribution of polar nanoregions observed by PFM. This leads us to exclude the A-sites vacancies as the origin of the local fields leading to the random distribution of polar nanoregions.

Figure 4(a) shows the XPS survey spectrum for the SBN surface after annealing at 700 °C. The C 1s peak is below the detection limit showing that the surface is clean. The Ba $3d_{5/2}$, Sr 3d, Nb 3d, and O 1s core level spectra are shown in Figs. 4(b)–4(e) at normal and 60° (more surface sensitive) emission. No new chemical states are observed with respect to XPS data acquired after annealing at lower temperature or as-received. The XPS spectra were fitted using CasaXPS software,[19] Gaussian-Lorentzian lineshapes, and Shirley background. The Sr 3d spin-orbit (S-O) splitting was fixed at 1.8 eV and the intensity ratio of the S-O doublet to 1.5. The sensitivity factors in the NIST database[20] were used to estimate stoichiometry.

The Ba $3d_{5/2}$ spectra have only one main component with a binding energy (BE) of 779.8 eV. Bulk and surface spectra are identical; the single peak is therefore assigned to Ba in A2 sites with unchanged occupancy in the surface and near-surface region.

The Sr 3d spectra are presented in Fig. 4(c). There are two 3d doublets. The first, at low binding energy (LBE) of 133.8 eV ($3d_{5/2}$) is labelled 1, the second, is shifted by 1.2 eV to high binding energy (HBE) and labelled 2. The grazing emission spectrum shows that this LBE component is slightly more intense at the surface. The A1 and A2 sites have different chemical environments because they are 12 and 15-fold oxygen coordinated and provide a straightforward explanation for the two components. We therefore attribute Sr1 to Sr in the A1 site and Sr2 to Sr in the A2 site. This agrees both qualitatively and quantitatively with a recent XPS study of SBN.[21]

The surface stoichiometry, as deduced from the XPS peak areas is $Sr_{0.63}Ba_{0.37}Nb_2O_{5.972}$, in agreement with that deduced from bulk sensitive XRD and close to that obtained from the dielectric measurements. The slight difference in Sr 3d intensities at normal and 60° emission may be due to some surface oxygen vacancies (V_O) at the surface, however, as will be discussed below, the concentration involved is an order of magnitude lower than that required to justify the interpretation of the LBE component of the Sr 3d as a surface peak.

The Nb 3d spectra show no low binding energy (LBE) component which would be representative of reduced Nb, for example, Nb^{4+}, formed under oxygen-deficit conditions.[21] This is to be expected because lower Nb valence states oxidize to Nb^{5+} at room temperature.[22,23]

The O 1s spectra in Fig. 4(e) have three components, peak 1 at 529.8 eV, due to oxygen in the perovskite-like environment, and peaks 2 (530.8 eV) and 3 (531.9 eV). The latter are clearly of surface origin (their relative intensity doubles at an emission angle of 60°). From the binding energies, peak 2 may be attributed to oxygen in lattice positions coordinated with a proton,[15] whereas peak 3 is ascribed to hydroxyl groups chemically bound to surface cations,[24] present even in some dry samples.[25]

From the relative intensities of the Ba and Sr 3d core-levels, we determine a [Sr]/[Ba] ratio of 1.67 using Sr (Ba) cross-sections and inelastic mean free paths of 0.06934

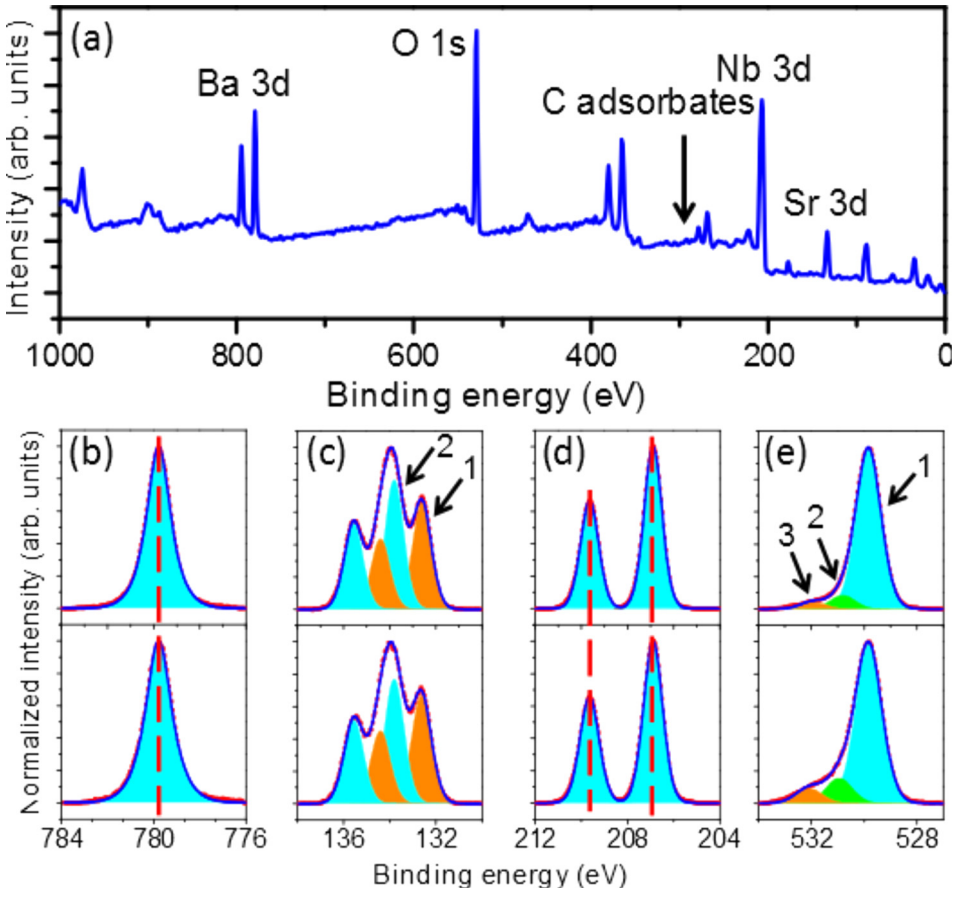

FIG. 4. (a) XPS survey spectrum of SBN(001) single crystal. Core level spectra: (b) Ba $3d_{5/2}$; (c) Sr 3d; (d) Nb 3d; (e) O 1s core level spectra at normal (top) and 60° (bottom) emission angles.

(0.6036) and 1.78 (1.085) nm, respectively.[20] X-ray measurements give the A1 and A2 site occupancy to be 66%–72% and ~90%, respectively, whatever the Sr/Ba ratio.[12] For $Sr_{0.63}Ba_{0.37}Nb_2O_6$, the general structural formula can therefore be written as $[(Sr1)_{1.4}(Sr2)_{1.73}(Ba)_{1.87}][(Nb_{B1})_2(Nb_{B2})_8]O_{30}$. This gives a ratio of the Sr A-site occupancy, $[Sr]_{A2}/[Sr]_{A1} = 1.24$. The measured XPS intensity ratio is, however, 1.21 (1.15) for the bulk (surface). Identifying the Sr1 and Sr2 with the A1 and A2 sites, respectively, the $[Sr]_{A2}/[Sr]_{A1}$ ratio is therefore 2.1% (7.0%) less than that expected from stoichiometry. Although small, the difference is greater than the typical XPS sensitivity and therefore significant.

One possible explanation is a contribution to the SrI intensity from Sr in the A2 site reduced by electron transfer following formation of V_O. Such charge transfer would occur principally to Sr because of the larger Pauling electronegativity. The Sr intensity ratio could then be written: $([Sr]_2–2V_O)/([Sr]_1 + 2V_O) = 1.21(1.15)$, with $[Sr]_1 + [Sr]_2 = 0.63$ giving a bulk and surface V_O concentration of 0.14% and 0.47%, respectively. These low V_O values are consistent with the absence of states in the band gap (not shown). The UHV annealing may simply have redistributed Sr occupation of the A1 and A2 sites within the bounds described by Podlozhenov *et al*.[12] Long range ordering of cation vacancies, as suggested by the LEED patterns, would require cation mobility, making Sr redistribution possible.

An alternative interpretation of the LEED patterns could be some sort of surface segregation leading to reconstructions, often observed in the case of adsorbates.[17,18] However, the LEED patterns were always the same, even for the as-received sample (although much weaker). Furthermore, the Sr/Ba surface stoichiometry changes by less than 7% after annealing at 700 °C temperature and no new core level component is observed. We can therefore exclude a chemically different surface phase as being at the origin of the LEED reconstruction. The LEED patterns could also be due to the ordering of oxygen vacancies, particularly as the sample was annealed at 700 °C. However, this would require 1/6 oxygen vacancies which is 30 times greater than the estimated concentration. Therefore, the only possibility for the observed LEED patterns is A-site vacancy ordering.

In conclusion, XPS, XRD, and electrical characterization show reasonable agreement on the SBN stoichiometry. Well-defined $(\sqrt{5} \times \sqrt{5})R26.6°$ and $(5\sqrt{2} \times \sqrt{2})R45°$ surface reconstructions are observed and thought to be due to the long-range order of alkaline earth metal vacancies on A sites. The quantitative XPS analysis shows that stoichiometry is preserved at the surface, confirming that the cation vacancy ordering is consistent with the bulk SBN structure. The electron beam spot is ~0.1 mm. Therefore, the LEED shows ordering of the cation vacancy sites occurs over distances much greater than the polar regions observed by PFM, while the electrical measurements show that the dielectric constant has the typical relaxor behavior. This excludes cation vacancies from being at the origin of the relaxor behavior. Chernaya *et al*. provide evidence that the relaxor properties are closely linked to the displacement of Sr atoms off the mirror axis in the pentagonal A2 sites.[10] The splitting in the Ba and Sr positions decreases with increasing Sr content, increasing the relaxor behavior, and reducing the acentric distortion of the NbO_6 octahedra responsible for the purely ferroelectric properties.

This knowledge should be invaluable in predicting the ferroelectric properties of, for example, strain engineered thin films. Future work should include a systematic chemical analysis of the XPS peaks as a function of the Sr content and micro-probe LEED with sub-micron spatial resolution in order to map out the distribution of the surface reconstructions and study the correlations with the nano-polar regions.

This work was supported by the French National Research Agency (ANR) project Surf-FER, ANR-10-BLAN-1012.

[1]L. Van Uitert, J. Rubin, and W. Bonner, IEEE J. Quantum Electron. **4**, 622 (1968).
[2]U. B. Dörfler, R. Piechatzek, T. Woike, M. K. Imlau, V. Wirth, L. Bohatý, T. Volk, R. Pankrath, and M. Wöhlecke, Appl. Phys. B: Lasers Opt. **68**, 843 (1999).
[3]P. V. Lenzo, E. Spencer, and A. Ballman, Appl. Phys. Lett. **11**, 23 (1967).
[4]M. D. Ewbank, R. R. Neurgaonkar, W. K. Cory, and J. Feinberg, J. Appl. Phys. **62**, 374 (1987).
[5]M. Horowitz, A. Bekker, and B. Fischer, Appl. Phys. Lett. **62**, 2619 (1993).
[6]M. Cuniot-Ponsard, J. M. Desvignes, A. Bellemain, and F. Bridou, J. Appl. Phys. **109**, 014107 (2011).
[7]P. B. Jamieson, S. Abrahams, and J. Bernstein, J. Chem. Phys. **48**, 5048 (1968).
[8]K. Tanaka, O. Nakagawara, M. Nakano, T. Shimuta, H. Tabata, and T. Kawai, Jpn. J. Appl. Phys., Part 1 **37**, 6142 (1998).
[9]V. Shvartsman, W. Kleemann, T. Ukasiewicz, and J. Dec, Phys. Rev. B **77**, 054105 (2008).
[10]T. S. Chernaya, B. A. Maksimov, T. R. Volk, L. I. Ivleva, and V. I. Simonov, Phys. Solid State **42**, 1716 (2000).
[11]A. Belous, O. Vyunov, D. Mishchuk, S. Kamba, and D. Nuzhnyy, J. Appl. Phys. **102**, 014111 (2007).
[12]S. Podlozhenov, H. A. Graetsch, J. Schneider, M. Ulex, M. Wöhlecke, and K. Betzler, Acta Crystallogr., Sect. B: Struct. Sci. **62**, 960 (2006).
[13]W. Kleemann, J. Mater. Sci. **41**, 129 (2006).
[14]T. Woike, V. Petíček, M. Dušek, N. K. Hansen, P. Fertey, C. Lecomte, A. Arakcheeva, G. Chapuis, M. Imlau, and R. Pankrath, Acta Crystallogr., Sect. B: Struct. Sci. **59**, 28 (2003).
[15]J. L. Wang, F. Gaillard, A. Pancotti, B. Gautier, G. Niu, B. Vilquin, V. Pillard, G. L. M. P. Rodrigues, and N. Barrett, J. Phys. Chem. C **116**, 21802 (2012).
[16]C. David, T. Granzow, A. Tunyagi, M. Whlecke, T. Woike, K. Betzler, M. Ulex, M. Imlau, and R. Pankrath, Phys. Status Solidi A **201**, R49 (2004).
[17]M. Borg, A. Mikkelsen, M. Birgersson, M. Smedh, E. Lundgren, D. L. Adams, C.-O. Almbladh, and J. N. Andersen, Surf. Sci. **515**, 267 (2002).
[18]A. Jaworowski, R. Ásmundsson, P. Uvdal, and A. Sandell, Surf. Sci. **501**, 74 (2002).
[19]N. Fairley, see http://www.casaxps.com/.
[20]*NIST Electron Inelastic-Mean-Free-Path Database- Version 1.2*, edited by C. J. Powell and A. Jablonski (National Institute of Standards and Technology, Gaithersburg, 2010).
[21]C. S. Dandeneau, Y. Yang, B. W. Krueger, M. A. Olmstead, R. K. Bordia, and F. S. Ohuchi, Appl. Phys. Lett. **104**, 101607 (2014).
[22]V. Atuchin, I. Kalabin, V. Kesler, and N. Pervukhina, J. Electron Spectrosc. Relat. Phenom. **142**, 129 (2005).
[23]P. Singh, B. J. Brandenburg, C. P. Sebastian, D. Kumar, and O. Parkash, Mater. Res. Bull. **43**, 2078 (2008).
[24]J. D. Baniecki, M. Ishii, T. Shioga, K. Kurihara, and S. Miyahara, Appl. Phys. Lett. **89**, 162908 (2006).
[25]S. Wendt, J. Matthiesen, R. Schaub, E. K. Vestergaard, E. Lægsgaard, F. Besenbacher, and B. Hammer, Phys. Rev. Lett. **96**, 066107 (2006).